CHAPTER 4

RESULTS AND DISCUSSION

4.1 Raw Materials Properties

In this research, main combustible fractions of MSW (paper, biomass, and plastic) were investigated, as single component and in the form of RDF. Raw materials were obtained locally from the same source; (i) office paper was chosen as a representative of the paper fraction, (ii) bamboo was chosen as a representative of the biomass fraction and (iii) polyethylene (PE) taken from transparent plastic bottles was chosen to represent the plastic fraction. As for the pyrolysis experiments, bamboo and PE were prepared into small pieces with diameter of 2 mm and length of 20 mm. A number of bamboo and PE pieces were banded by wire. Paper was mashed, and compacted into a cylindrical mold with diameter of 20 mm and length of 40 mm, after drying in an oven at 90^{o}C for 48 h. Simulated RDF consisted of 30% paper, 20%wt PE, and 50%wt bamboo. All of raw materials were mashed, mixed, and compacted into a cylindrical mold with 20 mm in diameter and 40 mm long, after drying in an oven at 90^{o}C for 48 h. Each sample mass was about 5 ± 0.1 g. While data for PE was taken from a published report (Mastellone et al., 2002), proximate analyses of RDF, its other components, and chars were carried out in this work by thermogravimetric method using a Perkin Elmer, model TGA7 instrument. Ultimate analyses were carried out by dynamic flash combustion method using a ThermoQuest, model Flash EA 1112 CHNS-O analyzer.

Results of the compositional analyses of the RDF and its main components were summarized in Table 4.1.

Table 4.1 Properties of raw materials

Properties	Quantity						
	Waste paper		Bamboo		PE	RDF	
	Raw	Char	Raw	Char	Raw	Raw	Char
Proximate analysis (% wt)							
Moisture	3.19	1.96	5.7	3.10	0.00[a]	3.29	1.6
Volatile	83.19	14.43	74.7	12.21	99.48[a]	83.43	11.56
Fixed carbon	4.53	54.96	14	72.03	0.17[a]	11.71	60.69
Ash	9.09	28.65	5.6	9.66	0.35[a]	2.26	24.46
Ultimate analysis (% wt)							
Carbon	43.54	83.55	45.6	87.20	84.63[a]	48.07	84.33
Hydrogen	6.24	1.62	4.3	1.35	14.41[a]	6.3	1.68
Oxygen	50.16	14.81	49.7	10.43	0.23[a]	45.4	13.98
Nitrogen	0.06	0.01	0.24	0.01	0.04[a]	0.23	0.01
Sulphur	0	0	0	0	0.00[a]	0	0
H/C molar ratio	1.708	0.231	1.124	0.322	2.03	1.56	0.237
O/C molar ratio	0.865	0.133	0.818	0.090	0.002	0.709	0.124
N/C molar ratio	0.0012	0.0001	0.0045	0.0001	0.0004	0.0041	0.0001
Empirical formula	$CH_{1.708}O_{0.865}N_{0.0012}$	$CH_{0.231}O_{0.133}N_{0.0001}$	$CH_{1.124}O_{0.818}N_{0.0045}$	$CH_{0.322}O_{0.090}N_{0.0001}$	$CH_{2.030}O_{0.002}N_{0.0004}$	$CH_{1.560}O_{0.709}N_{0.0041}$	$CH_{0.237}O_{0.124}N_{0.0001}$
HHV (MJ/kg)	20.10[b]	38.54[b]	20.60[b]	40.52[b]	46.19[a]	22.34[b]	38.94[b]

[a] ; Mastellone et. al, (2002),

[b] ; From calculation (Moreno et. al, 2012)

4.2 Electric Field and Plasma Modeling Results

In this thesis, a laboratory scale, plasma reactor was designed and constructed, based on atmospheric microwave plasma generated from a commercially available 800 W continuous power input magnetron and a high voltage transformer. The electric field concentration is the key in this model as they are main parameters of the plasma system, designed in this thesis. Computer program used to calculate electric field and electron temperature. Electric field simulation was numerically carried out to show energy density distribution in the reactor. From preliminary simulation result, the energy field concentration was found to be around the center of the quartz tube. The plasma can only ignite in that region. The microwave energy density absorbed by plasmas was magnified around the reaction tube. Simulation results of a 800 W microwave plasma reactor in this thesis were electric field in the oven cavity and electron temperature in the reaction zone. Microwave radiation generated electric filed in the oven cavity. Electric field was calculated in frequency transient mode. It was found to concentrate at the reaction zone in the quartz tube. This simulation results indicated the best location of the reaction tube for this design. The maximum value of electric field in the reaction zone was about 7 kV/m at the time of 1×10^{-7} s, as shown in Figure 4.1. From electric field simulation results, a plasma can be generated in quartz reaction tube. Electron temperature of a plasma was calculated. The maximum electron temperature in the reaction zone at the argon flow rate of 0.50, 0.75, 1.00, and 1.25 lpm were not difference. It was maximum at 23,557 K at the time of 1×10^{-7} s, as shown in Figure 4.2. Preliminary experimental runs confirmed that the plasma was successfully generated with our reactor. It was shown that sufficiently large volume of plasma can be established in the reactor.

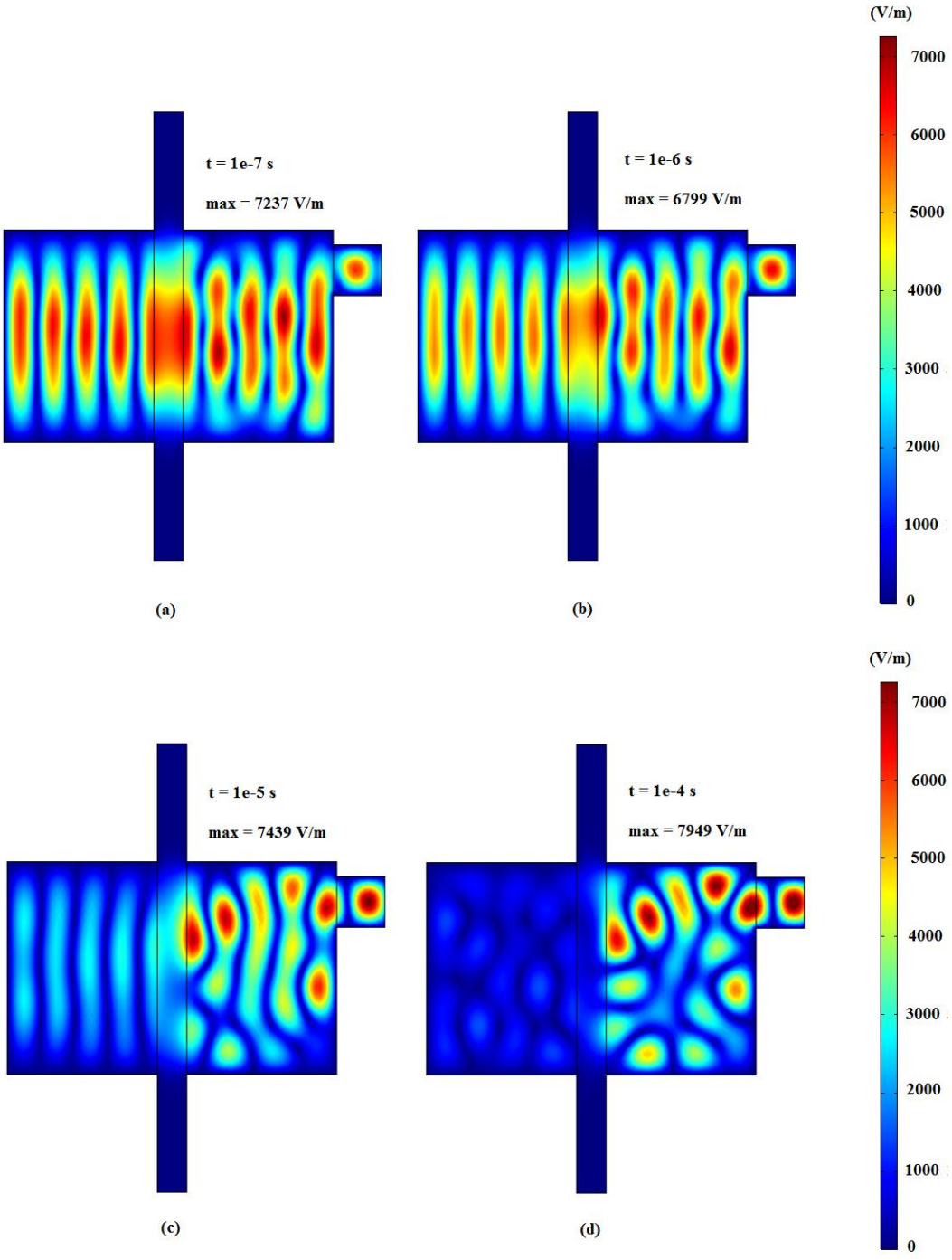

Figure 4.1 Electric field in the oven cavity

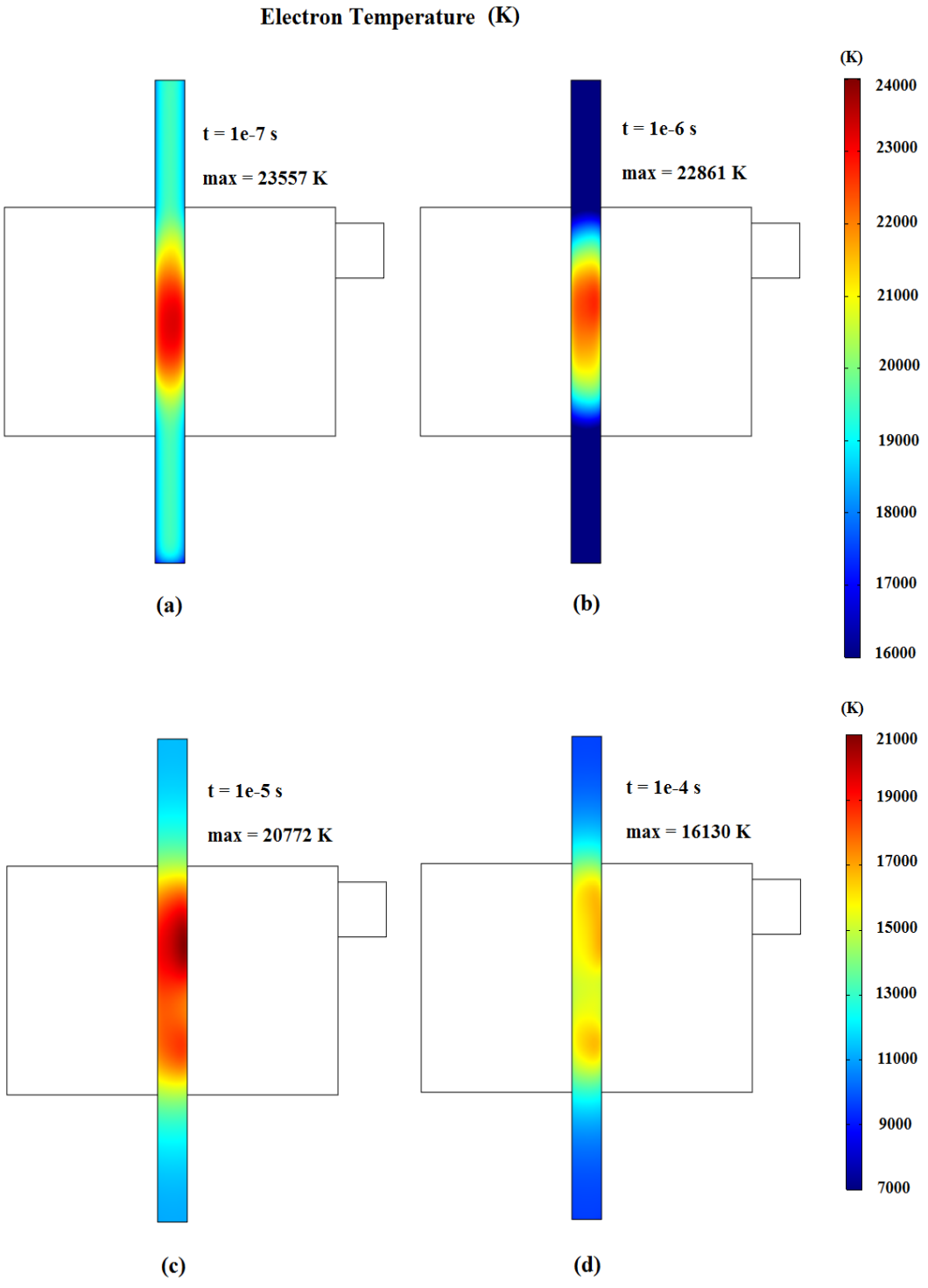

Figure 4.2 Electron temperature

4.3 Plasma Characteristics

When the microwave reactor was switched on, a pinkish plasma flame was observed in an empty tube. A small bluish yellow flame was observed at the start of conversion process, if there was a feedstock present in the tube. This observation may be a result of partial oxidation and release of volatile matter from the feedstock. For different carrier gas flow rates, the post gas temperature measured at 20 mm away from the top of discharge zone inside the quartz tube was found to be 1063 – 1536 K. The discharge length was derived from measurements of the discharge images captured by a digital camera. It was averaged in the range of 45-72 mm. The plasma was stabilized along discharge length inside the quartz reaction tube with cross section area of 5.7 cm^2. For the range of flow rates considered (0.50 – 1.25 lpm), residence time, defined as plasma volume divided by the respective flow rate, was between 1.9 – 2.8 s. Power density was calculated to be around between 19 – 35 W/cm^3. A summary of the plasma characteristics under variable carrier gas flow rate was shown in Table 4.2. The post gas temperature showed initial increase with increasing carrier gas flow rate, reaching averaged maximum at 1536 K for 0.75 lpm argon flow rate, as shown in Figure 4.3. Further increases in argon supply led to reduction in the temperature. The observed decline in post gas temperature at higher flow rates may be attributed to; (i) the low flow rates of the carrier gas generated the plasma with short discharge length. Its volume was too small, compared with the feed stock size. The energetic particle concentration in the low flow rate was not enough, therefore the rate of its electrons collision was decreased that affected to plasma generation, (ii) increasing carrier gas flow rate increased the discharge length and volume, and resulted in decreasing power density and residence time, and (iii) in this

research, the extra high flow rate generated the non-stabilized plasma, the breakdown of electromagnetic field was occasionally observed, as a result of plasma temperature changes (Karches et al., 2001). Plasma flame characteristics and post gas temperature were shown in Figure 4.4.

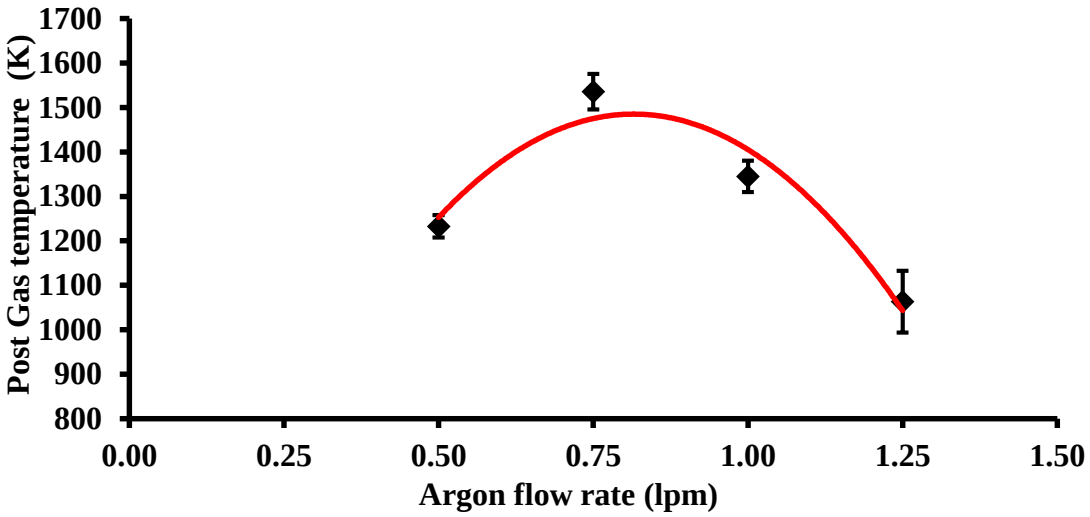

Figure 4.3 Post Gas temperature

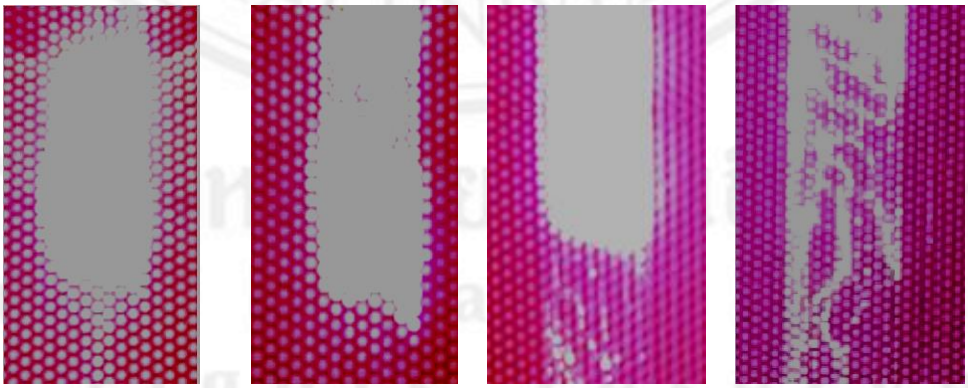

(a) (b) (c) (d)

Figure 4.4 Plasma flame characteristic, (a) Ar flow rate 0.50 lpm, (b) Ar flow rate 0.75 lpm, and (c) Ar flow rate 1.00 lpm, and (d) Ar flow rate 1.25 lpm

Table 4.2 Microwave plasma characteristics

Flow rate (lpm)	Temperature (K)	Discharge length (cm)	Power density (W/cm^3)
	1231	4.5	31.2
0.50	1259	4.0	35.1
	1208	5.0	28.1
Average	1233	4.5	31.4
SD	26	0.5	3.5
	1531	5.0	28.1
0.75	1498	5.5	25.5
	1578	5.0	28.1
Average	1536	5.2	27.2
SD	40	0.3	1.5
	1373	5.5	25.5
1.00	1305	5.5	25.5
	1357	6.0	23.4
Average	1345	5.7	24.8
SD	36	0.3	1.2
	1073	7.0	20.1
1.25	989	7.0	20.1
	1127	7.5	18.7
Average	1063	7.2	19.6
SD	70	0.3	0.8

4.4 Gas Product

The product gas obtained from the plasmochemical process was collected and measured. Major gas components generated were CO, H_2, CH_4, CO_2 and O_2. The most important gas species to consider for plasmochemical processes were H_2, CO, and CH_4. The results show that there were some differences between the raw materials. When paper and biomass were used as feedstock, it was possible to produce a high heating value syngas with high H_2 content exceeding maximum at 24% and 22%, respectively. Whereas, when plastic was used as feedstock, syngas with low H_2 content and high CO and CO_2 contents was produced may be due to the fact that

hydrogen and carbon contents in raw materials are the resulted in product gas components. The product gas composition was shown in Table 4.3, gas yields and heating values of product gas were also shown in Table 4.4, respectively. Average heating value and gas yield of product gas of all feedstock were 10.48 MJ/m^3 and 1.38 m^3/kg, respectively. Although present in the detected product gas, other detected fraction would not be taken into account due to their low contents. A majority was undesirable tars. The product gas obtained from the plasma reaction was collected and measured. Major gas components generated were H_2, CO, CO_2, CH_4, and O_2, respectively.

4.4.1 Effect of Carrier Gas Flow Rate on Evolution of Product Gas

Figures. 4.3-4.6 show effect of carrier gas flow rate on evolution of product gas. Within the range of flow rates considered, average total content of combustible fractions in the product gas of all feed stock was 79.76%, showing similar pattern to change in H_2, CO, and CH_4 contents with argon flow rate. CH_4 was not found to vary significantly with argon flow, it remained relatively stable at 1.60-3.69% for all feedstock. H_2 and CO appeared to exhibit more pronounced change with respect to carrier gas flow rate. They were found to initially increase with increasing argon flow, reaching maximum value at flow rate of 0.75 lpm. After which, they were markedly reduced at higher carrier gas supply rate may be due to two reasons, that (i) the flow was too fast inside the reactor, hence, less likely for biomass material and the plasma to react with each other more completely, (ii) this flow rate generated maximum plasma flame temperature. In this research, the use of paper, biomass, plastic, and RDF as feedstock generated H_2 about 24%, 22%, 10%, and 14%, respectively. CO

was the most observed combustible fraction of product gas. It was found to be in the range between 56-73%.

Table 4.3 Product gas composition

Feed stock	Gas Composition (%mol)	Argon flow rate (lpm)				
		0.50	0.75	1.00	1.25	Average
Waste paper	H2	22.05	23.81	23.52	21.38	22.69
	CO	57.91	58.38	58.39	57.65	58.08
	CO2	14.71	12.15	12.70	15.72	13.82
	CH4	3.38	4.36	3.98	3.05	3.69
	O2	1.94	1.29	1.41	2.20	1.71
	Sum	100	100	100	100	100
	Combustible fraction	83.35	86.56	85.88	82.09	84.47
Biomass	H2	18.98	22.42	20.19	18.04	19.91
	CO	54.53	55.62	54.69	49.11	53.49
	CO2	19.68	15.45	17.89	24.64	19.41
	CH4	2.91	3.69	3.56	3.21	3.34
	O2	3.91	2.82	3.67	5.01	3.85
	Sum	100	100	100	100	100
	Combustible fraction	76.41	81.72	78.44	70.36	76.73
PE	H2	6.78	9.48	8.88	6.05	7.80
	CO	66.52	72.61	70.59	65.69	68.85
	CO2	19.64	11.93	14.21	19.55	16.33
	CH4	1.63	1.77	1.55	1.46	1.60
	O2	5.43	4.21	4.77	7.24	5.41
	Sum	100	100	100	100	100
	Combustible fraction	74.93	83.86	81.02	73.20	78.25
RDF	H2	10.87	13.79	13.75	10.71	12.28
	CO	63.32	65.47	63.77	62.11	63.67
	CO2	18.77	14.21	15.69	20.54	17.30
	CH4	3.63	3.99	3.78	3.21	3.65
	O2	3.40	2.53	3.00	3.44	3.09
	Sum	100	100	100	100	100
	Combustible fraction	77.82	83.25	81.30	76.02	79.60

Table 4.4 Yields and heating values of product gas

	Flow rate (lpm)	Gas yield ($N\text{-}m^3/kg$)	Gas LHV (MJ/m^3)
Waste Paper	0.50	1.03	10.89
	0.75	1.27	11.49
	1.00	1.39	11.32
	1.25	1.42	10.67
	Average	1.28	11.09
Biomass	0.50	1.29	9.96
	0.75	1.61	10.75
	1.00	1.83	10.35
	1.25	1.98	9.28
	Average	1.68	10.08
PE	0.50	1.13	9.70
	0.75	1.45	10.81
	1.00	1.67	10.41
	1.25	1.90	9.45
	Average	1.54	10.09
RDF	0.50	0.85	10.46
	0.75	1.01	11.17
	1.00	1.08	10.88
	1.25	1.11	10.13
	Average	1.01	10.66

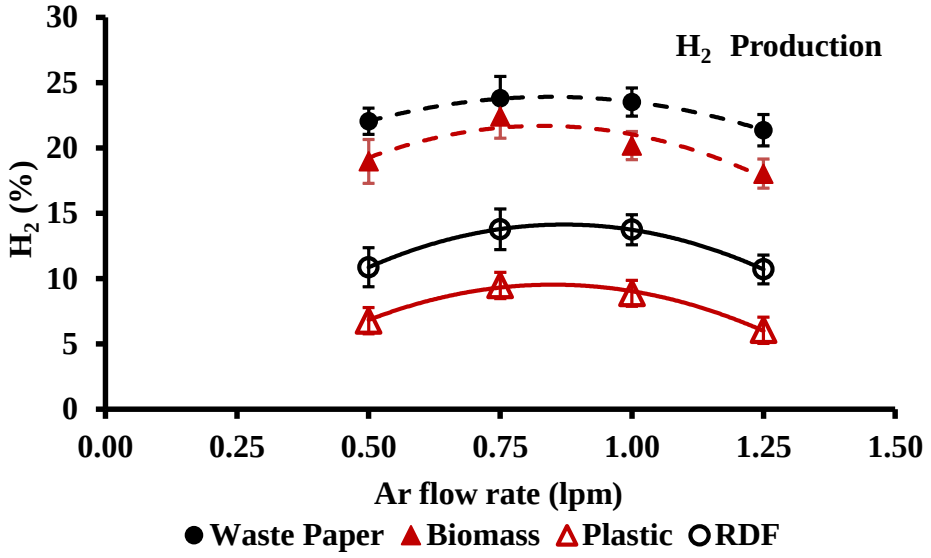

Figure 4.5 Variation of H_2 evolution with carrier gas flow rate and type of feedstock

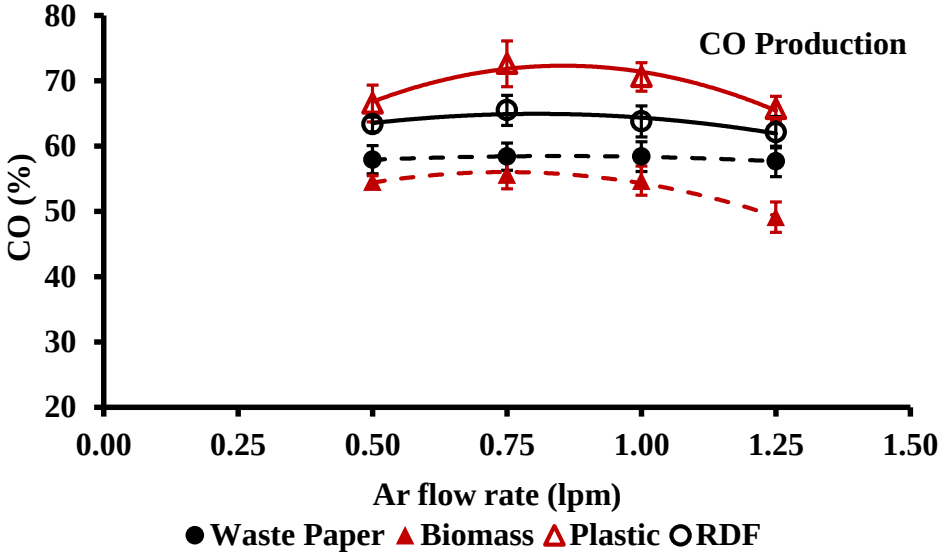

Figure 4.6 Variation of CO evolution with carrier gas flow rate and type of feedstock

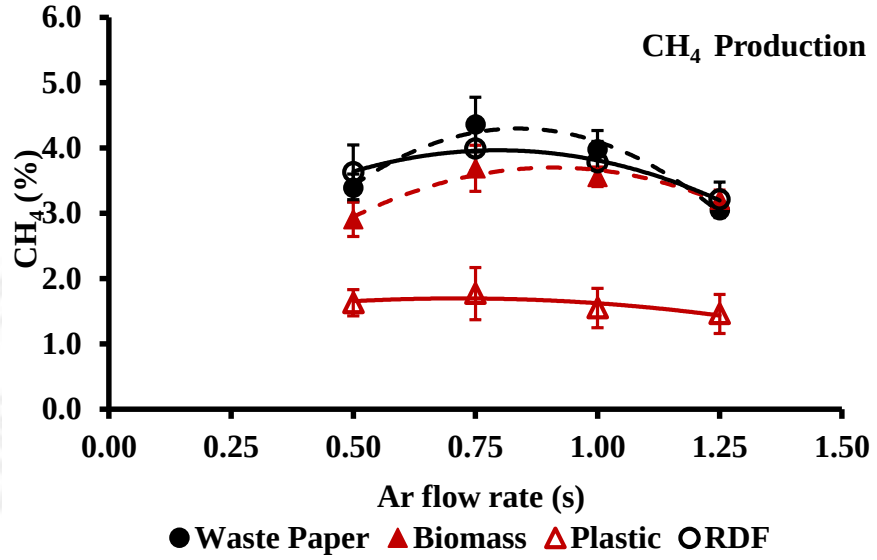

Figure 4.7 Variation of CH_4 evolution with carrier gas flow rate and type of feedstock

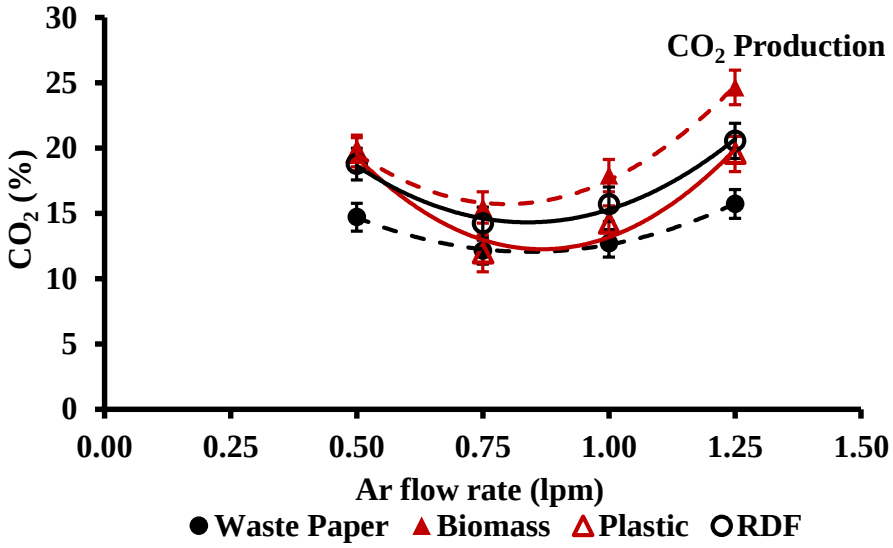

Figure 4.8 Variation of CO_2 evolution with carrier gas flow rate and type of feedstock

4.4.2 Effect of Residence Time on Evolution of Product Gas

Figures. 4.9 to 4.12 show effect of residence time on evolution of syngas. Within the range of residence time, showing similar pattern to change in H_2, CO, and

CH_4 contents with residence time. CH_4 was not found to vary significantly with residence time, H_2 and CO appeared to exhibit more pronounced change with respect to residence time. They were found to initially increase with increasing residence time, reaching maximum value at residence time of 2.25 s. After which, they were markedly reduced at higher residence time may be due to three reasons, that (i) the low residence time, less likely for biomass material and the plasma to react with each other more completely, and the extra high flow rate generated the non-stabilized plasma (ii) this residence time (2.25 s) generated maximum plasma flame temperature, (iii) high residence time, the low flow rates of the carrier gas generated the plasma with short discharge length. Its volume was too small, compared with the feed stock size. The energetic particle concentration in the low flow rate was not enough, therefore the rate of its electrons collision was decreased that affected to plasma generation.

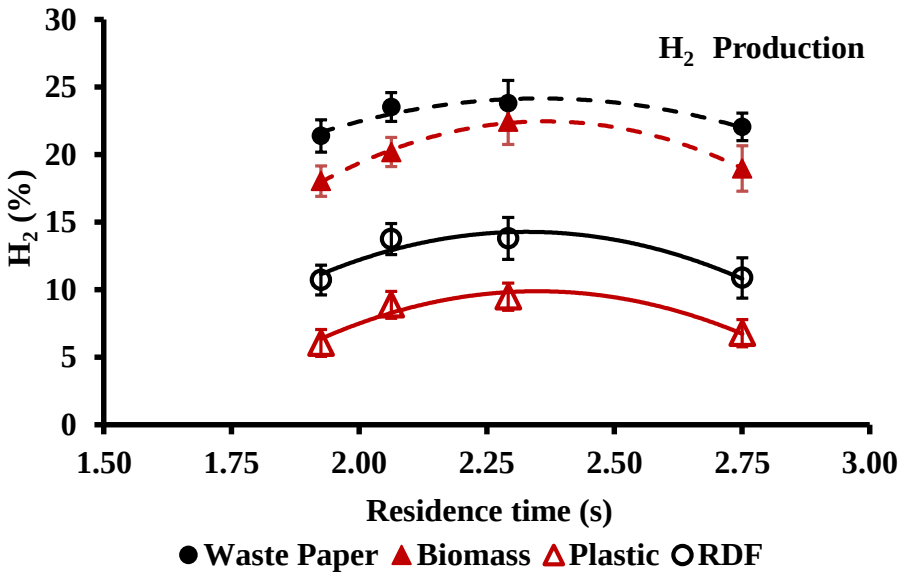

Figure 4.9 Variation of H_2 evolution with residence time and type of feedstock

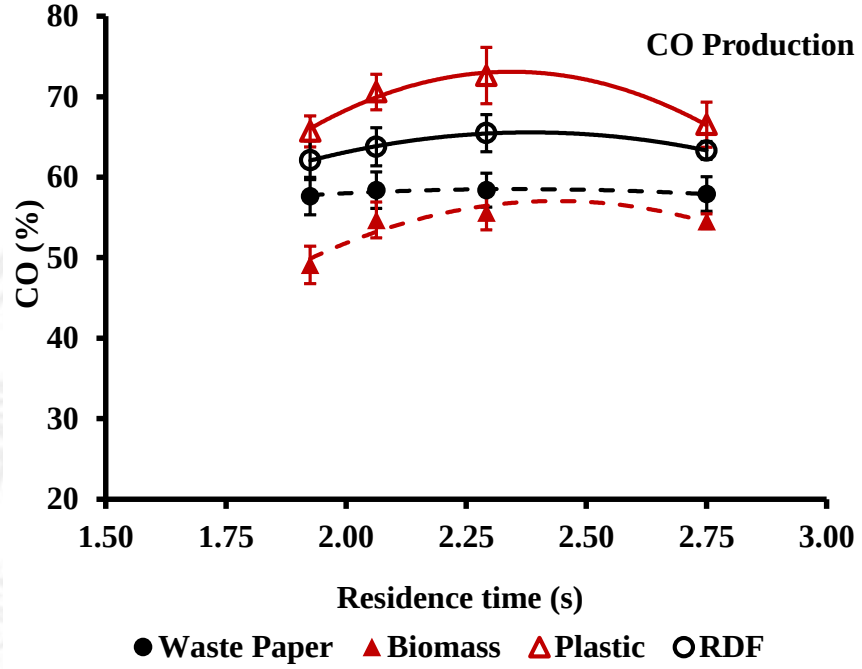

Figure 4.10 Variation of CO evolution with residence time and type of feedstock

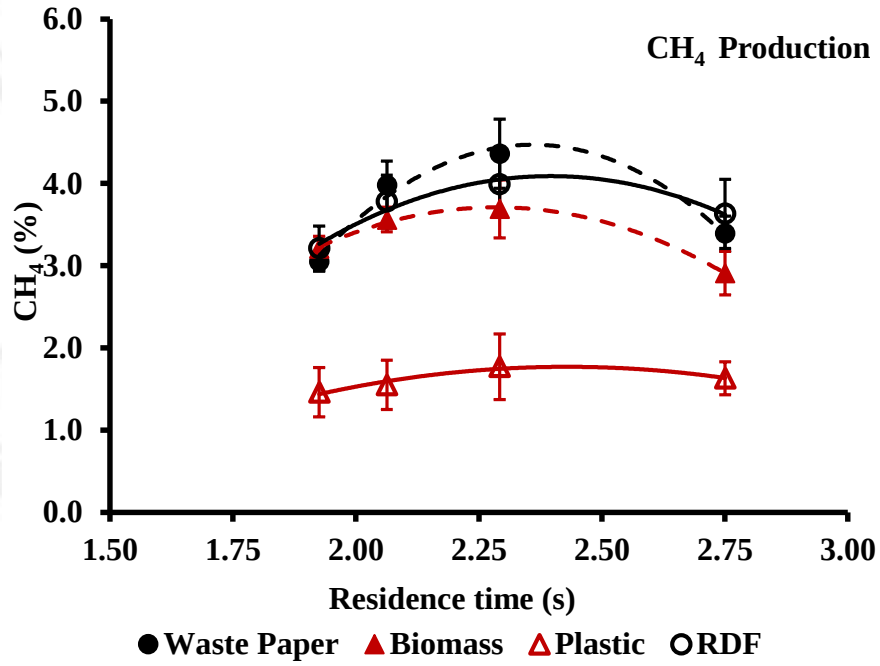

Figure 4.11 Variation of CH_4 evolution with residence time and type of feedstock

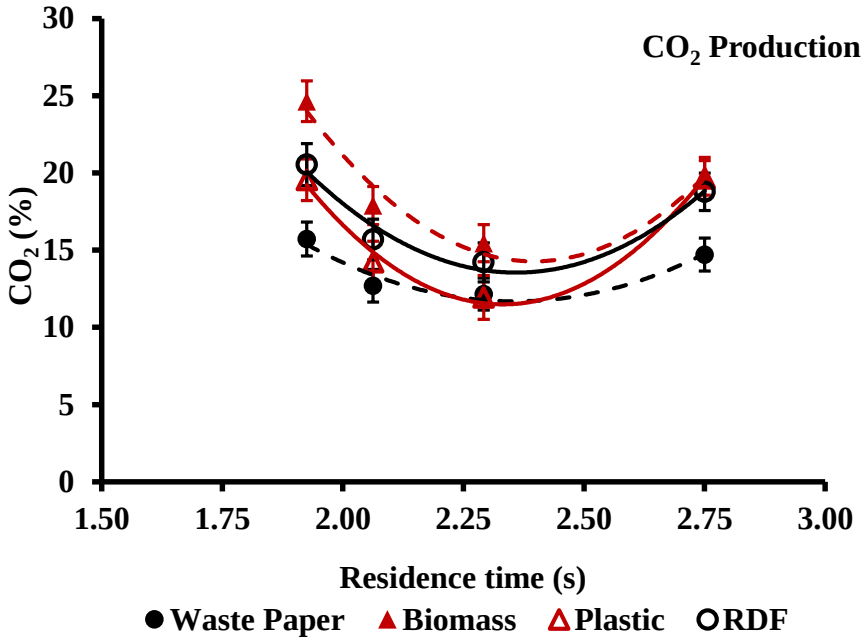

Figure 4.12 Variation of CO_2 evolution with residence time and type of feedstock

4.5 Char Products

Char characteristics and yield are important in evaluating the performance of the plasma reactor (Ouensanga et. al, 2003), The proximate and ultimate analyses and calorific value of the char obtained from the plasma pyrolysis are also shown in Table 4.5. The fixed carbon of chars was found to significantly increase, compared to that original in the starting materials. Significant degree of carbonization appeared to take place under non-thermal plasma environment. The ultimate analysis gives the compositions in mass concentration of carbon, hydrogen, oxygen, nitrogen and sulphur. Increase in carbon content in the resulting char was in line with proximate analysis result. The char yields of paper, biomass, plastic, and RDF were listed in Table 4.6. They were averaged about 21%, 12%, 18% and 16%, respectively. Average carbon conversion efficiency were about 78%, 83%, 78% and 79%, respectively.

HHV of the chars of paper, biomass, and RDF were about 39%, 41%, and 39 MJ/kg, respectively.

4.6 Mass Balance

In this research, the mass of feedstock (m_{feed}) was preweighted before every experiments. The products are gas, solid and liquid residual. The gas volume (V_{gas}) was measured by the gas meter. The mass of gas (m_{gas}) was calculated using equation (3.7). The averaged product gas mass of waste paper, biomass, PE, and RDF were 3.72 g, 2.51 g, 2.30 g, and 6.02 g, respectively. The product gas mass of all feedstock were found to initially increase with increasing argon flow, reaching maximum value at flow rate of 0.75 lpm. After which, they were markedly reduced at higher carrier gas supply rate may be due to two reasons, that (i) the flow was too fast inside the reactor, hence, less likely for biomass material and the plasma to react with each other more completely, (ii) this flow rate generated maximum plasma flame temperature. In this research, the use of waste paper, biomass, plastic, and RDF as feedstock generated product gas mass about 73%w/w, 83%w/w, 76%w/w, and 75%w/w, respectively. The product of plasmochemical conversion of RDF is gas, char, and liquid, they were averaged about 75%w/w, 16%w/w, and 9%w/w, respectively. Mass balanced of plasmochemical products were summarized in Table 4.7.

Table 4.5 Fuel properties of char products

Feed Stock	Moisture	Volatile matter	Fixed carbon	Ash	C	H	O	N	S	HHV (MJ/kg)
Paper	2.0	14.4	54.9	28.6	83.6	1.6	14.8	0.01	0	38.5
Biomass	3.1	12.2	72.0	9.7	87.2	1.4	10.4	0.01	0	40.5
RDF	1.6	11.6	60.7	24.5	84.3	1.7	14.0	0.01	0	38.9

Table 4.6 Char yields and carbon conversion efficiency

	Flow rate (lpm)	Char yield (%)	Carbon conversion (%)
Waste Paper	0.50	22.05	75.94
	0.75	19.14	84.14
	1.00	21.43	80.63
	1.25	21.33	70.85
	Average	20.99	77.89
Biomass	0.50	10.32	84.17
	0.75	11.94	89.77
	1.00	12.00	85.88
	1.25	13.79	71.81
	Average	12.01	82.91
PE	0.50	16.77	76.65
	0.75	16.13	84.78
	1.00	18.33	77.91
	1.25	20.69	70.81
	Average	17.98	77.54
RDF	0.50	15.70	77.12
	0.75	15.57	82.43
	1.00	15.68	79.99
	1.25	15.43	75.31
	Average	15.59	78.71

Table 4.7 Mass balance of plasmochemical products

	Flow rate (lpm)	Mass (%w/w)		
		Gas	Char	Liquid
Waste Paper	0.50	73.3	22.4	4.3
	0.75	78.0	19.2	2.8
	1.00	74.1	21.2	4.7
	1.25	68.1	21.4	10.5
	Average	73.4	21.0	5.6
Biomass	0.50	84.4	10.3	5.3
	0.75	86.8	11.9	1.3
	1.00	84.9	12.0	3.1
	1.25	75.1	13.8	11.1
	Average	82.8	12.0	5.2
PE	0.50	76.3	16.8	6.9
	0.75	80.0	16.1	3.9
	1.00	75.0	18.3	6.7
	1.25	72.0	20.7	7.3
	Average	75.8	18.0	6.2
RDF	0.50	74.5	15.7	9.8
	0.75	77.0	15.6	7.4
	1.00	75.9	15.7	8.4
	1.25	73.7	15.4	10.9
	Average	75.3	15.6	9.1

4.7 Energy Analysis

In this thesis, energy efficiency was defined as Output energy from gas product divided by microwave input energy. Microwave input energy was calculated from microwave input power 800 W multiplied by reaction time 3 min. It was 0.144 MJ. Output energy is the energy from gas product. It was calculated from the mass of feedstock (m_{feed}), yield (Y_{gas}) and calorific value (LHV) of product gas. The averaged energy efficiency plasmochemical conversion of waste paper, biomass, PE, and RDF were about 50%, 35%, 32%, and 60%, respectively. The energy efficiency were found to initially increase with increasing argon flow, reaching maximum value at flow rate of 1.0 lpm. After which, they were slightly reduced at higher carrier gas supply rate may be due to two reasons, that (i) this flow rate generated gas product with calorific value close to maximum (at flow rate of 0.75 lpm) and high yield, (ii) at higher flow rate, calorific value of gas product was markedly reduced. Maximum energy efficiency of plasmochemical conversion of RDF was about 66%, and energy from gas product was 0.095 MJ. The energy efficiency of plasmochemical conversion of all feedstock in this research were summarized in Table 4.8.

Table 4.8 Energy efficiency

Feedstock	Flow rate (lpm)	Feedstock (g)	Gas yield (N-m^3/kg)	Gas LHV (MJ/m^3)	Gas Energy (MJ)	Energy eff. (%)
Paper	0.50	5.0	1.05	10.89	0.057	39.70
	0.75	5.1	1.27	11.49	0.074	51.68
	1.00	5.1	1.37	11.32	0.079	54.93
	1.25	5.1	1.42	10.67	0.077	53.66
	Average	5.08	1.28	11.09	0.072	49.99
Biomass	0.50	3.1	1.29	9.96	0.040	27.66
	0.75	3.1	1.61	10.75	0.054	37.26
	1.00	3.0	1.83	10.35	0.057	39.46
	1.25	2.9	1.98	9.28	0.053	37.00
	Average	3.03	1.68	10.08	0.051	35.35
PE	0.50	3.1	1.13	9.7	0.034	23.60
	0.75	3.1	1.45	10.81	0.049	33.74
	1.00	3.0	1.67	10.41	0.052	36.22
	1.25	2.9	1.9	9.45	0.052	36.16
	Average	3.03	1.54	10.09	0.047	32.43
RDF	0.50	7.9	0.85	10.46	0.070	48.78
	0.75	7.9	1.01	11.17	0.089	61.89
	1.00	8.1	1.08	10.88	0.095	66.10
	1.25	8.1	1.11	10.13	0.091	63.25
	Average	8.00	1.01	10.66	0.086	60.00

4.8 Thermodynamic Equilibrium Modeling Results

The comparison of product gas compositions between thermodynamic equilibrium modeling and experiment results from plasmochemical conversion of

waste paper, biomass, and RDF were shown in Figures 4.13 to 4.25. The model calculated too low CO_2 yields and too high H_2 and CH_4 than the experiments. The other gas compositions were similar value for all feedstock. In order to make a model more accurate, the model have been adjusted for each feedstock by adding the constants. It was found that the adjusted model had corrected RMSE. Compared RMSE between model and adjusted model with experiment were shown in Table 4.9.

Table. 4.9 RSME of model

Gas	Waste Paper	Biomass	RDF
	RMSE	RMSE	RMSE
CO	1.13	1.46	0.96
CO2	4.3	6.27	6.92
CH4	2.1	1.43	0.81
H2	1.32	1.95	1.43
RMSE	2.55	3.44	3.59

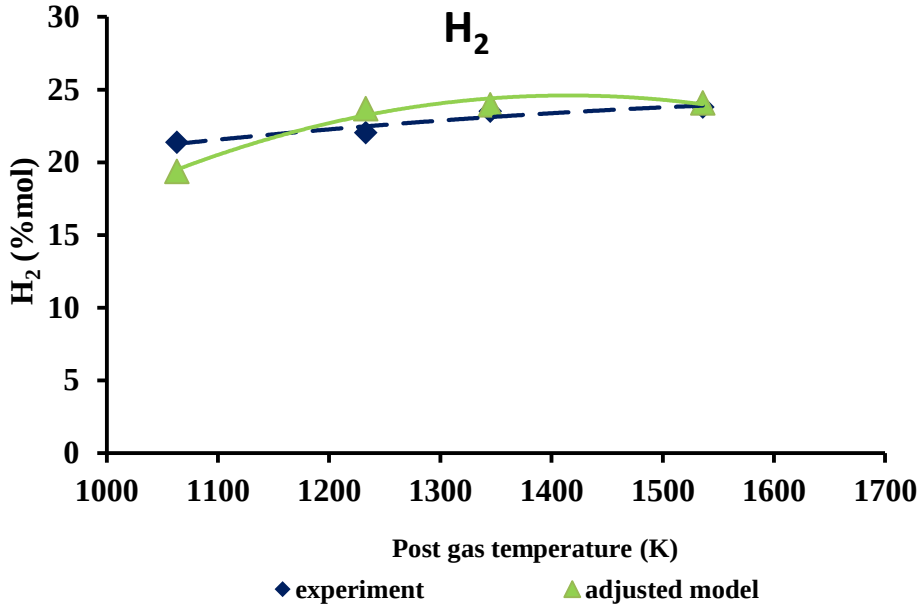

Figure 4.13 H_2 concentration in product gas of waste paper,

compared experimental result with thermodynamic equilibrium modeling

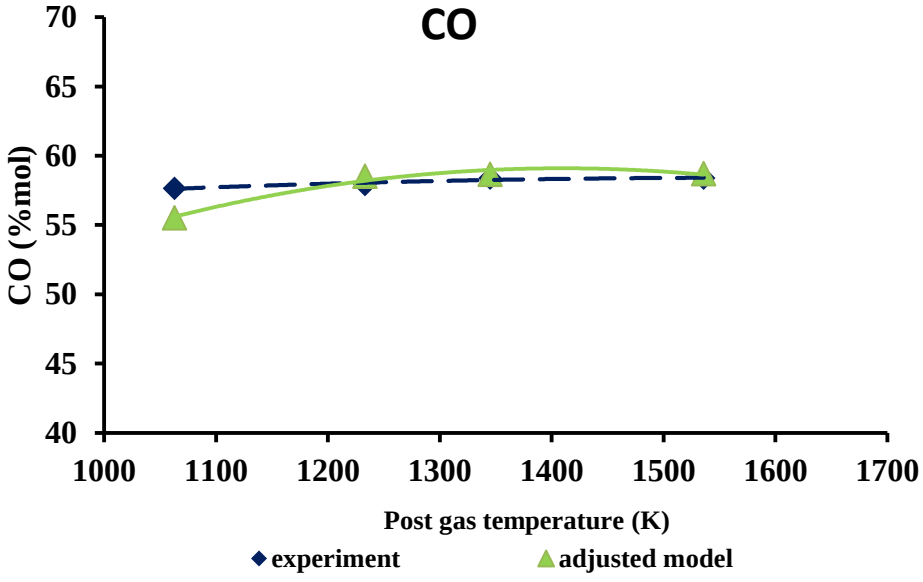

Figure 4.14 CO concentration in product gas of waste paper,

compared experimental result with thermodynamic equilibrium modeling

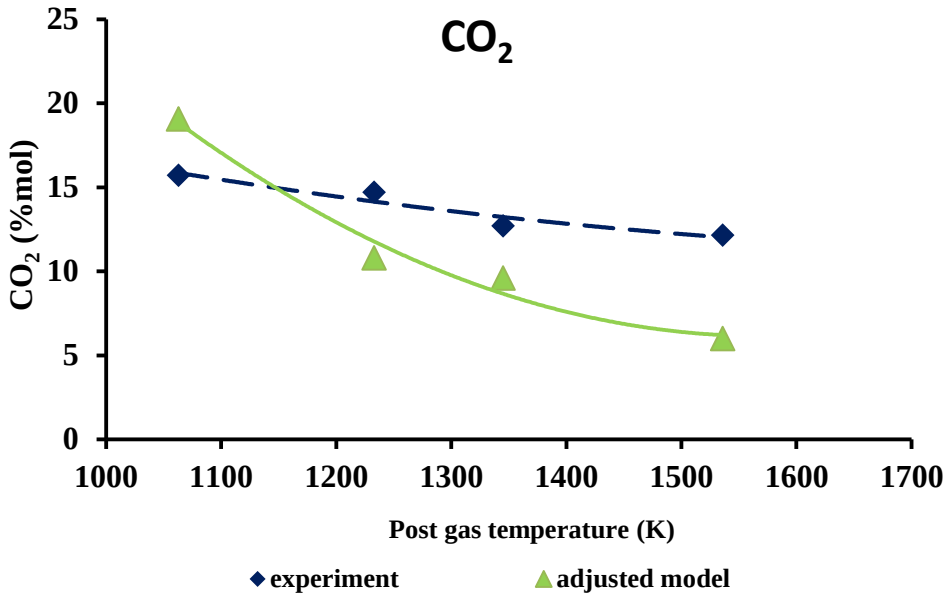

Figure 4.15 CO_2 concentration in product gas of waste paper,

compared experimental result with thermodynamic equilibrium modeling

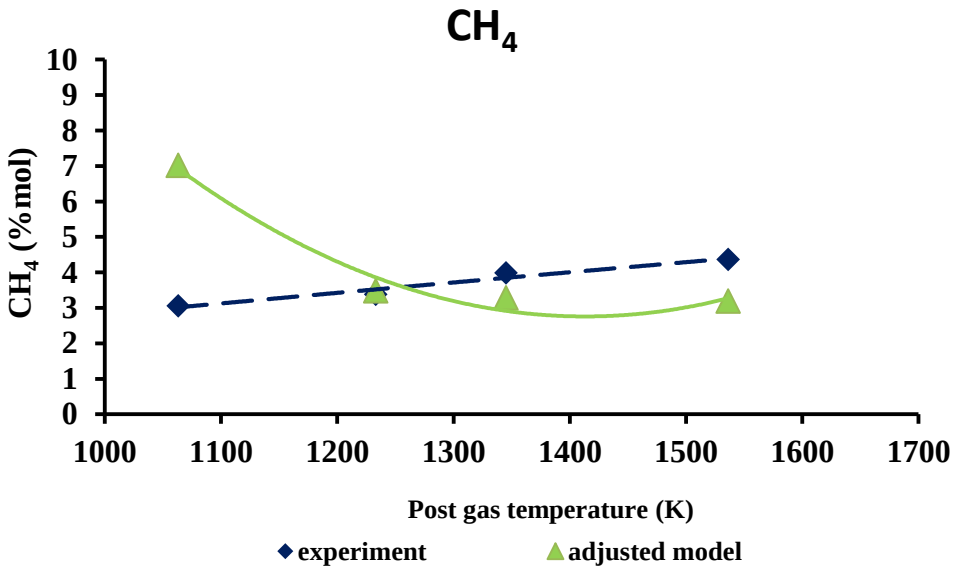

Figure 4.16 CH_4 concentration in product gas of waste paper,

compared experimental result with thermodynamic equilibrium modeling

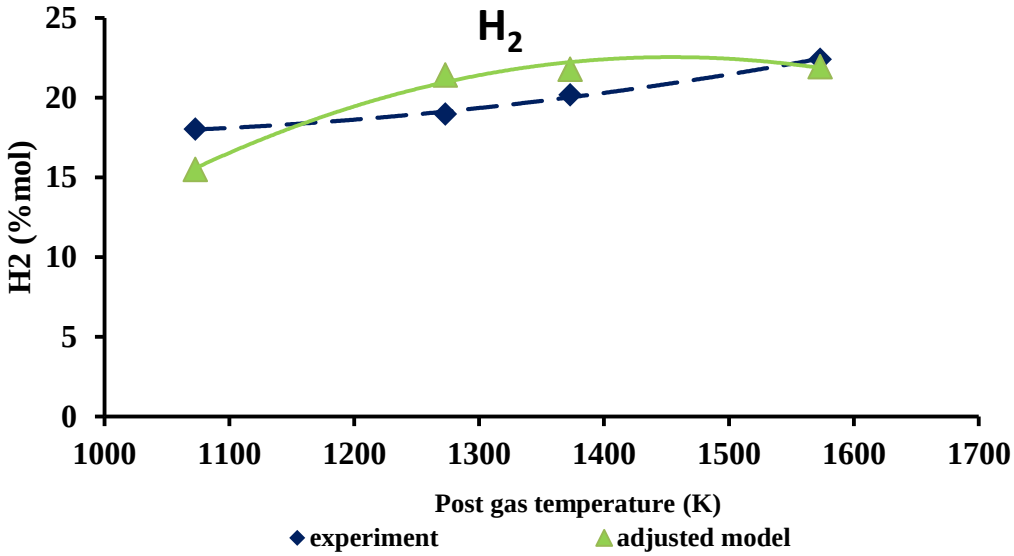

Figure 4.17 H_2 concentration in product gas of biomass,

compared experimental result with thermodynamic equilibrium modeling

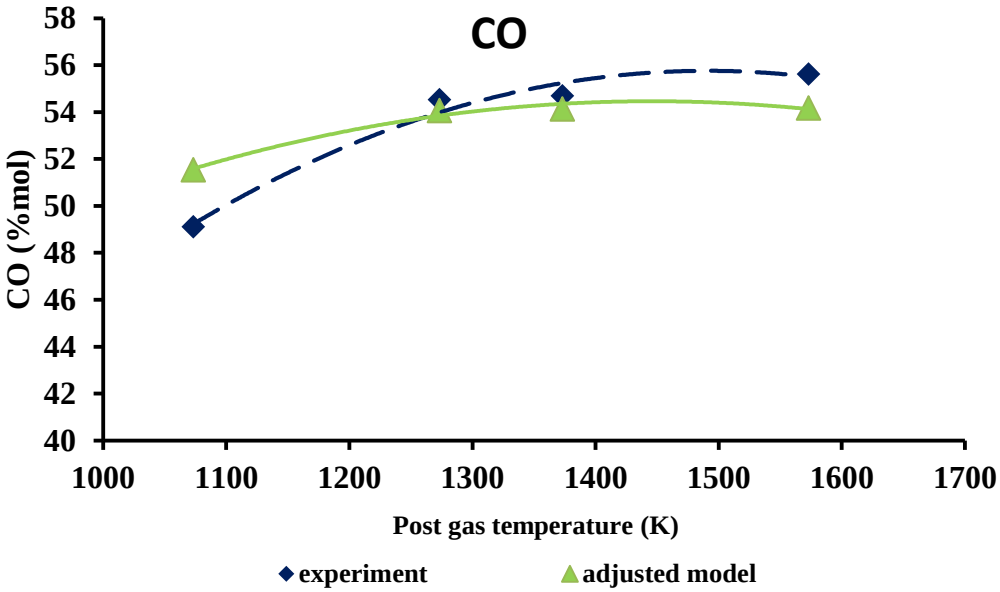

Figure 4.18 CO concentration in product gas of biomass,

compared experimental result with thermodynamic equilibrium modeling

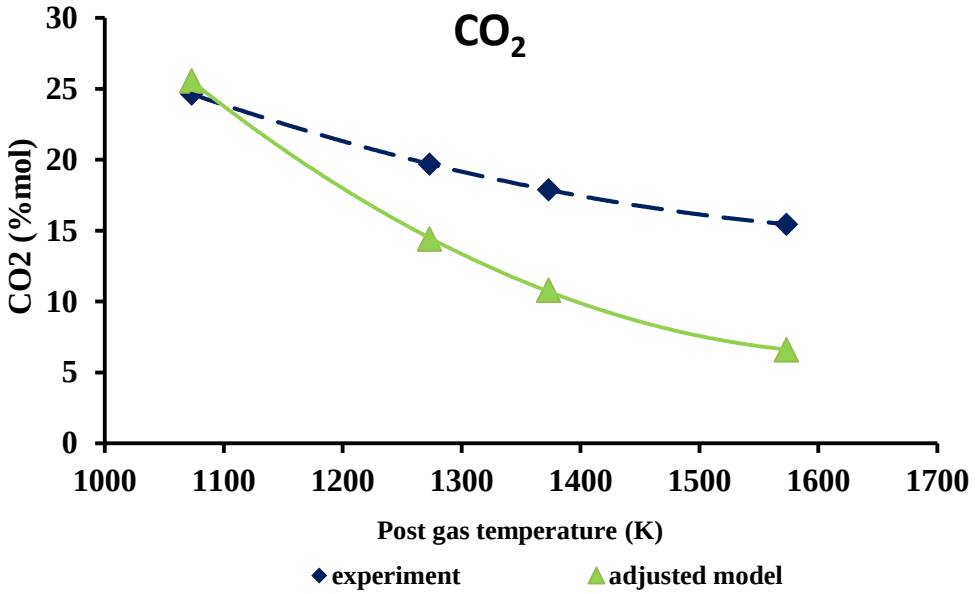

Figure 4.19 CO_2 concentration in product gas of biomass,

compared experimental result with thermodynamic equilibrium modeling

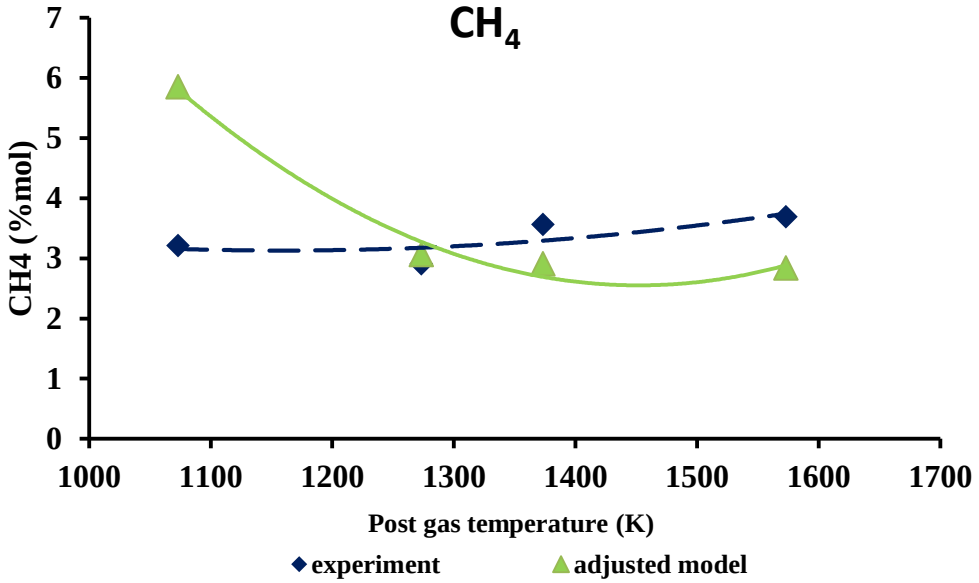

Figure 4.20 CH_4 concentration in product gas of biomass,

compared experimental result with thermodynamic equilibrium modeling

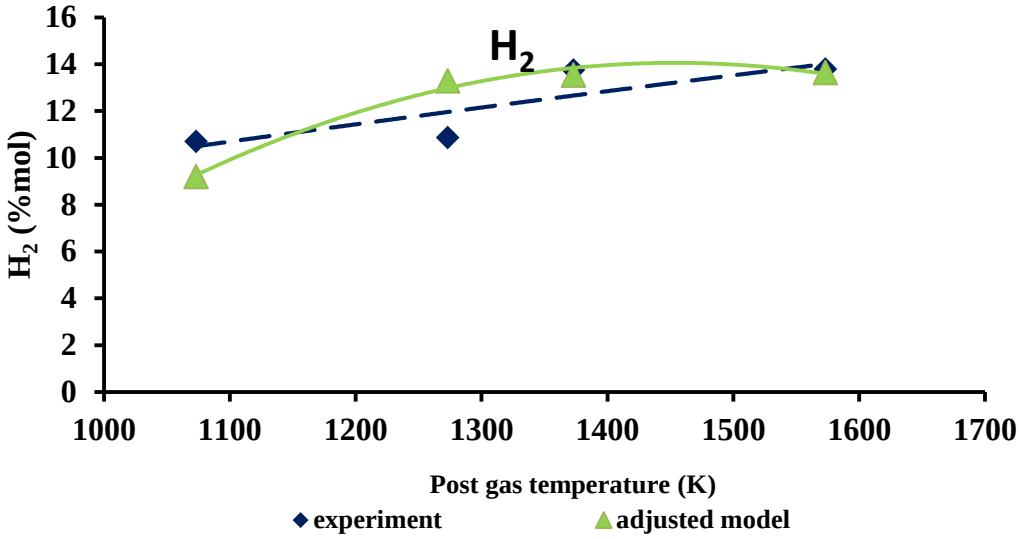

Figure 4.21 H_2 concentration in product gas of RDF,

compared experimental result with thermodynamic equilibrium modeling

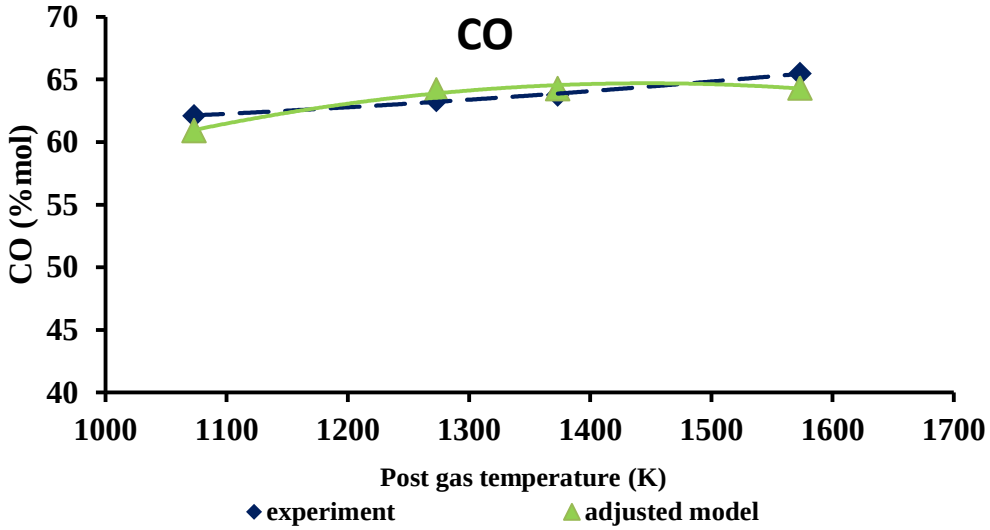

Figure 4.22 CO concentration in product gas of RDF,

compared experimental result with thermodynamic equilibrium modeling

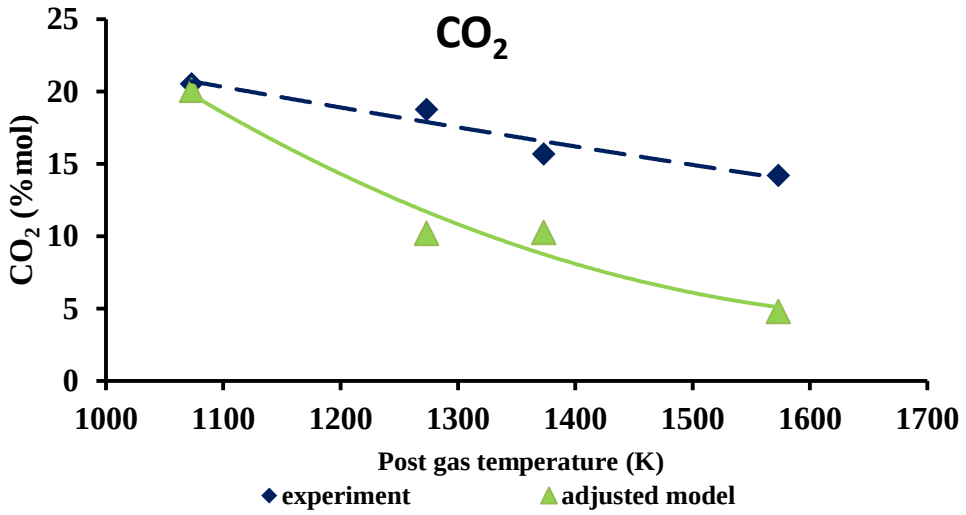

Figure 4.23 CO_2 concentration in product gas of RDF,

compared experimental result with thermodynamic equilibrium modeling

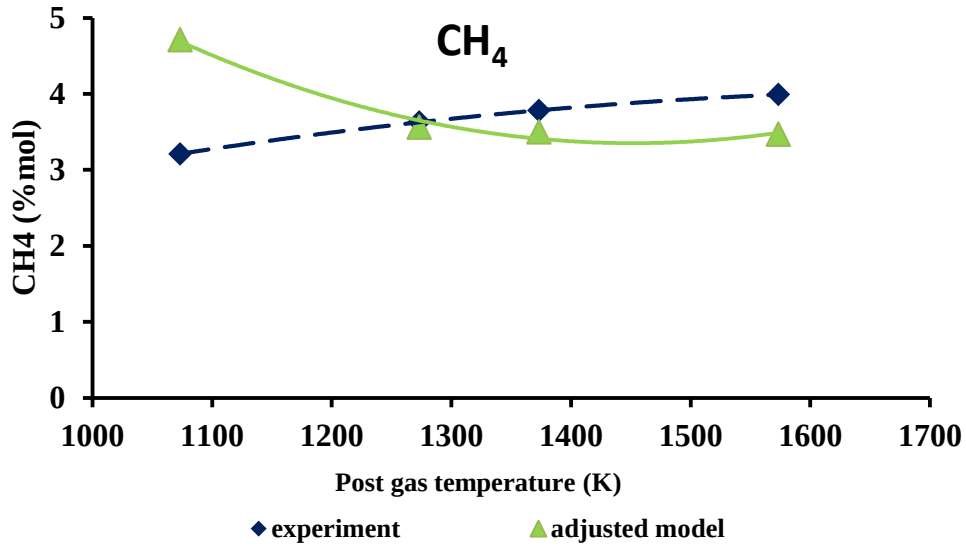

Figure 4.24 CH_4 concentration in product gas of RDF,

compared experimental result with thermodynamic equilibrium modeling

4.9 Comparison with Literatures

Elemental analyses results of RDF used as feedstock in this research were compared with literature. Product gas from plasma pyrolysis of paper, biomass, plastic, and RDF in this research were compared against those obtained from other types of feedstock and plasma sources and conditions. Against microwave plasma pyrolysis of waste wood (Lupa et al., 2012), the product gas heating value from microwave plasma pyrolysis of bamboo in this work was in similar magnitude, but with higher H_2 and CH_4 contents. In comparison with thermal plasma assisted pyrolysis of sawdust (Tang et al., 2005), the products gas in this work showed higher gas heating value, H_2 and CH_4 contents, but lower char yield. The comparison is summarized in Tables 4.10 to 4.11.

Table 4.10 Comparison of char between this work and the literatures

Reference	Method	Feedstock	Char	
			Yield (%)	HHV (MJ/kg)
This work	Microwave plasma	RDF	15.6	38.9
		Biomass	12.0	40.5
		Paper	21.0	38.5
		PE	18.0	-
Wang et al., 2012	Microwave plasma	Rice husk	33.4	21.6
	Microwave plasma	Cane residue	25.5	27.8
Tang et al., 2005	RF Plasma	Sawdust	33.3	29.0
Tang et al., 2004	DC arc discharge plasma	Used tires	69.6	-
Zhao et al., 2012	Microwave pyrolysis	Wheat straw	46.3-56.2	-
Shie et al., 2010	Arc plasma torch	Rice straw	7.5-13.8	-

Table 4.11 Comparison of product gas between this work and the literatures

Reference	Method	Feedstock	Product gas content (%mol)				LHV (MJ/kg)
			H_2	CO	CH_4	CO_2	
This work	Microwave plasma	RDF	13.8	65.5	4.0	14.2	11.2
		Biomass	22.4	55.6	3.7	15.5	10.8
		Paper	23.8	58.4	4.4	12.2	11.5
		PE	9.5	72.6	1.8	11.9	10.8
Blanco et al., 2012	Sand bed pyrolysis	RDF	18.7	27.1	20.6	20.6	12.8
Kanilo et al., 2003	Microwave plasma	Coal	2.4	8.1	1.2	9.6	1.7
Zhao et al., 2012	Microwave plasma	Wheat straw	22.1	34.7	7.9	33.8	9.6
Sekiguchi et al., 2004	Microwave plasma	PE	14.0	26.0	6.0	12.0	6.9
Lupa et al., 2012	Microwave plasma	Wood	0.0	56.9	0.5	33.8	7.3
Kowalska et al., 2008	Gliding arc	Waste oil	0.0	0.5	0.0	2.0	0.1
Tang et al., 2005	RF plasma	Sawdust	8.5	11.0	1.5	4.0	2.8
Janajreh et al., 2013	Arc plasma	MSW	43.5	34.5	0.01	0.03	9.0